Geophysical Applications of Partial Wavelet Coherence and Multiple Wavelet Coherence

ERIC K. W. NG AND JOHNNY C. L. CHAN

Guy Carpenter Asia Pacific Climate Impact Centre, School of Energy and Environment, City University of Hong Kong, Hong Kong, China

(Manuscript received 16 March 2012, in final form 21 June 2012)

ABSTRACT

In this paper, the application of partial wavelet coherence (PWC) and multiple wavelet coherence (MWC) to geophysics is demonstrated. PWC is a technique similar to partial correlation that helps identify the resulting wavelet coherence (WTC) between two time series after eliminating the influence of their common dependence. MWC, akin to multiple correlation, is, however, useful in seeking the resulting WTC of multiple independent variables on a dependent one. The possible El Niño–Southern Oscillation–related impact of the large-scale atmospheric factors on tropical cyclone activity over the western North Pacific is used as an example. A software package for PWC and MWC has been developed. It also includes modified software that rectified the bias in the wavelet power spectrum and wavelet cross-spectrum. The package is available online (see http://www.cityu.edu.hk/gcacic/wavelet).

1. Introduction

The technique of wavelet analysis has increasingly become a common tool for time series examinations. It not only helps overcome the limitations of Fourier transform in analyzing nonstationary time series, but also tackles the problem of constant window width and thus the time-resolution issue over frequencies (Daubechies 1992). This is done by decomposing the time series into a time–frequency space with multi-time-resolution, which allows one to determine the dominant modes of variability and the change of those modes with time (Torrence and Compo 1998). It is very useful in the field of geophysics, in which trends and periodicities of oscillations with various frequencies are often studied.

Many studies have been carried out previously on the application of wavelet analysis to geophysics and some free toolkits have also been provided. For example, Torrence and Compo (1998) gave an excellent guide with a user-friendly toolkit for wavelet transform. Maraun and Kurths (2004) presented the evolution of cross-wavelet transform, developed a statistical test for wavelet coherence (WTC),[1] and discussed some pitfalls in wavelet applications. Extending the toolkit of Torrence and Compo (1998), Grinsted et al. (2004) provided a software package for cross-wavelet transform and WTC.

Recently, Mihanović et al. (2009) introduced two additional wavelet analysis techniques—partial wavelet coherence (PWC) and multiple wavelet coherence (MWC)—to the field of marine science for calculating the resulting WTC of two effects after eliminating their common dependent factor and the proportion of WTC that can be explained by multiple independent variables on one dependent, respectively. Ng and Chan (2012) applied PWC to remove the El Niño–Southern Oscillation (ENSO) effect, revealing the unlikely dependence of tropical cyclone intensity on local sea surface temperature in the Bay of Bengal.

While the PWC and MWC techniques should have wide applications in the study of geophysical systems, Mihanović et al. (2009) applied them only to extract oscillations with a particular frequency as a time series. The direct usage of these techniques in the frequency–time space, which is believed to be as valuable, has not

Corresponding author address: Eric Ng, School of Energy and Environment, Guy Carpenter Asia-Pacific Climate Impact Centre, City University of Hong Kong, Tat Chee Ave., Kowloon, Hong Kong, China.
E-mail: e.ng@student.cityu.edu.hk

DOI: 10.1175/JTECH-D-12-00056.1

[1] A list of acronyms and symbols used in this paper is available in the appendix.

yet been well documented. The present paper therefore aims to contribute toward such documentation by demonstrating the use of PWC and MWC in frequency–time space. Moreover, a Matlab software package for these techniques is developed, which also includes modified software [based on the program of Torrence and Compo (1998) and Grinsted et al. (2004)] that rectified the bias in the wavelet power spectrum (WPS) and wavelet cross-spectrum (Liu et al. 2007; Veleda et al. 2012).

Although several studies have suggested that the rise of sea surface temperature due to global warming may induce increases in tropical cyclone frequency and intensity (e.g., Knutson and Tuleya 1999; Emanuel 2005; Webster et al. 2005), Chan and Liu (2004) found that tropical cyclone activity over the western North Pacific (WNP) does not seem to depend on the rising sea surface temperature, though a large percentage of its variation is forced by large-scale atmospheric factors that are found to be associated with ENSO. The result is confirmed by Chan (2009). In this paper, an investigation using wavelet analysis of the ENSO-related impact of these large-scale atmospheric factors on tropical cyclone activity over the western North Pacific is conducted.

Section 2 contains the description of the ENSO example, data, and methodology used in this paper. Section 3 gives a summary review of the basics of wavelet analysis, including the continuous wavelet transform, cross-wavelet transform, phase angle, and WTC, which are necessary for a better understanding of the PWC and MWC methods. The PWC and MWC are then respectively introduced in sections 4 and 5, with their applications demonstrated. This paper is summarized with some discussions on wavelet applications in section 6.

2. Data and methodology

a. Tropical cyclone data

The tropical cyclone data of the International Best Track Archive for Climate Stewardship (IBTrACS; Knapp et al. 2010; Kruk et al. 2010) Project over the WNP during 1960–2008 are employed. The ratio of the number of typhoons to the number of tropical cyclones (RTY) is investigated in this study. Tropical cyclones and typhoons are only counted for maximum sustained wind speed when >34 and >64 kt, respectively, is reached in their lifetime.

b. Atmospheric data

The wind, temperature, geopotential height, and specific humidity data are from the reanalysis of the National Centers for Environmental Prediction–National Center for Atmospheric Research (Kalnay et al. 1996; see online at http://www.esrl.noaa.gov/psd/), which is of 2.5° latitude $\times$ 2.5° longitude horizontal resolution. Similar to Chan and Liu (2004), an empirical orthogonal function (EOF) is first performed via correlation matrices on the thermodynamic and dynamic parameters suggested by Gray (1979) that govern tropical cyclone genesis and development. The domain of 5°–30°N, 120°E–180° is selected, as tropical cyclones over the WNP mostly reach their maximum intensity south of 30°N and east of 120°E (Xue and Neumann 1984). Because over 90% of tropical cyclones in this region are recorded during May–November, only data from these months are used. The time series of the principal components (PCs) that are significantly correlated with that of RTY at a 95% confidence level and related to ENSO are then analyzed. The sign of the EOFs is chosen to give a positive correlation with ENSO.

c. The climatic oscillation indexes

The Niño-3.4 and Niño-3 indexes are extracted from the National Oceanic and Atmospheric Administration (NOAA) Earth System Research Laboratory website (http://www.esrl.noaa.gov/psd/data/climateindices/list). Both the Niño-3.4 and Niño-3 indexes are often used to detect the variability of the canonical ENSO.

Recently, an anomalous warming event similar to but different from the canonical ENSO has been found near the central Pacific; this phenomenon has been named the ENSO Modoki. The ENSO Modoki index (EMI) has been established to monitor its variability (Ashok et al. 2007). In this study, it is calculated from the NOAA Extended Reconstructed Sea Surface Temperature V3b dataset according to the definition

$$\mathrm{EMI} = [\mathrm{SSTA}]_C - 0.5[\mathrm{SSTA}]_E - 0.5[\mathrm{SSTA}]_W, \qquad (1)$$

where $[\mathrm{SSTA}]_C$, $[\mathrm{SSTA}]_E$, and $[\mathrm{SSTA}]_W$ are the sea surface temperature anomalies averaged over the regions (10°S–10°N, 165°E–140°W), (15°S–5°N, 110°–70°W), and (10°S–20°N, 125°–145°E), respectively.

The Indian Ocean dipole mode index (DMI) is extracted from the website of the Japan Agency for Marine-Earth Science and Technology (http://www.jamstec.go.jp/frcgc/research/d1/iod/).

3. Basic applications of wavelet analysis

a. Continuous wavelet transform

Wavelet transform is a tool often used for analyzing a nonstationary time series with different power at different frequencies. There are two types of wavelet transform—the continuous wavelet transform and discrete wavelet transform. Only the latter suits orthogonal wavelet bases, while both can be used for nonorthogonal

wavelet functions. Continuous wavelet transform is discussed in this paper.

By projecting a time series on a wavelet function $\psi_0(\eta)$, which must be time–frequency space localized and have zero mean, the decomposition makes it possible to obtain information from the local neighborhood. One frequently used wavelet function is the Morlet wavelet, which is also used in this paper as an example. Further, with convolution applied to a discrete sequence x_n and the scaled and translated wavelet, the continuous wavelet transform can be easily defined:

$$W_n^X(s) = \sqrt{\frac{\delta t}{s}} \sum_{n'=1}^{N} x_{n'} \psi_0 \left[(n' - n) \frac{\delta t}{s} \right], \qquad (2)$$

where $n = 1, \ldots, N$, s is the set of scales used, and δt is the time step (Grinsted et al. 2004). This transform could be calculated quicker via Fourier transform by doing N times the convolution given in (2) for each scale (Torrence and Compo 1998). WPS is defined as $2^j \times |W_n^X(s)|^2$, where j is the scale level and 2^j is multiplied so as to correct the bias toward low-frequency oscillations in the WPS. This bias has not been corrected in the programs offered by previous studies (Liu et al. 2007).

In general, either the white- or red-noise background spectrum is suitable for geophysical processes and hence used to define the null hypothesis for the significance test for peaks in WPS. Those phenomena of red-noise characteristics, like our example, can be well modeled by the lag-1 autoregressive process (Gilman et al. 1963; Allen and Smith 1996). With an appropriate background spectrum and desired confidence level, significant regions can be easily found.

While the WPSs of both the *monthly* Niño-3 and Niño-3.4 indexes (Fig. 1) are dominated at the period around the 2–7-yr band and do not appear to be very different, a slightly greater areal extent of significant regions is shown for the WPS of the Niño-3.4 index, particularly since 1980, when the ENSO Modoki started occurring more frequently. This could be because the Niño-3.4 index takes up signals from both the canonical ENSO and the ENSO Modoki given its geographical location, which has been suggested previously (Ashok et al. 2007; Chen and Tam 2010). We therefore use the Niño-3 index in this study to represent the canonical ENSO. Note that regions inside the cone of influence (COI; Torrence and Compo 1998), where discontinuities at end points occurred because of padding with zeros that may have distorted the results, are not considered.

b. Cross-wavelet transform and phase angle

A cross-wavelet transform helps compare two time series x_n and y_n by identifying their common power.

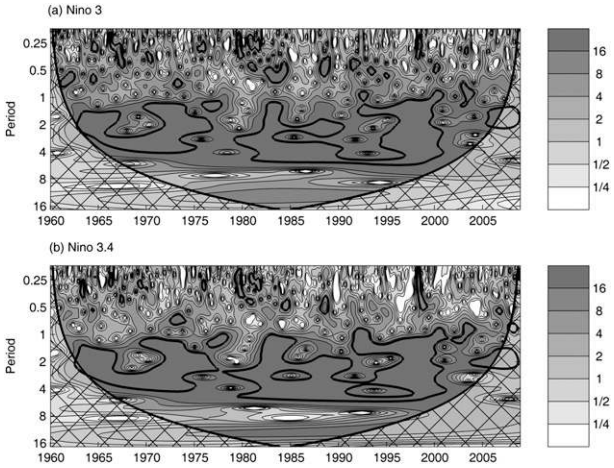

FIG. 1. The WPS of monthly (a) Niño-3 index and (b) Niño-3.4 index. Monthly climatological means of each month are removed from the datasets. The cross-hatching indicates regions inside the COI and the thick black contour indicates 95% confidence level, using red noise as background spectrum.

However, without normalizing to the single WPS, wavelet cross spectrum cannot completely reflect the possible link between two time series and is thus no longer useful for relationship identification, but it is for phase estimation. By decomposing the complex wavelet cross spectrum into cross-wavelet power $|W_n^{XY}(s)|$ and phase, one may write it as

$$W_n^{XY}(s) = |W_n^{XY}(s)| e^{i\Phi_n(s)}, \qquad (3)$$

where $\Phi_n(s)$ represents the phase difference at time t_n between the two signals (Maraun and Kurths 2004). Although a bias also exists in wavelet cross spectra like WPS does, the bias-correction method suggested by Veleda et al. (2012) for the cross-wavelet spectrum will not affect its imaginary part, and thus its usage in phase estimation. In this paper, phase angles pointing left and right represent antiphase and in-phase relationships, respectively. They may also be used for the verification of possible physical relationships. Consistent or slowly changing phase angles can be considered as evidence of significant relationships. The degrees in time units depend on the frequency band one is looking for. For example, 180° in a 1-yr frequency band represents a half-year. Examples demonstrating the combined usage of phase angles and WTC are provided in section 3c.

c. WTC

Wavelet coherence (WTC) is a tool for identifying possible relationships between two processes by searching frequency bands and time intervals during which they covary. In other words, WTC may enhance linear correlation analyses that help reveal intermittent correlations

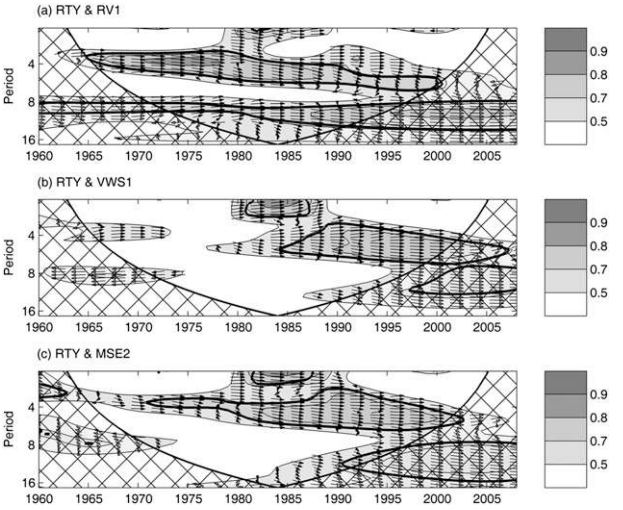

FIG. 2. The WTC of (a) RTY and RV1, (b) RTY and VWS1, and (c) RTY and MSE2 over the WNP during the period May–November. The cross-hatching indicates regions inside the COI and the thick black contour indicates 95% confidence level. The arrows indicate the relative phase relationship, with those pointing right representing in-phase, pointing left representing antiphase, and pointing straight down indicating the lead of RTY by 90°.

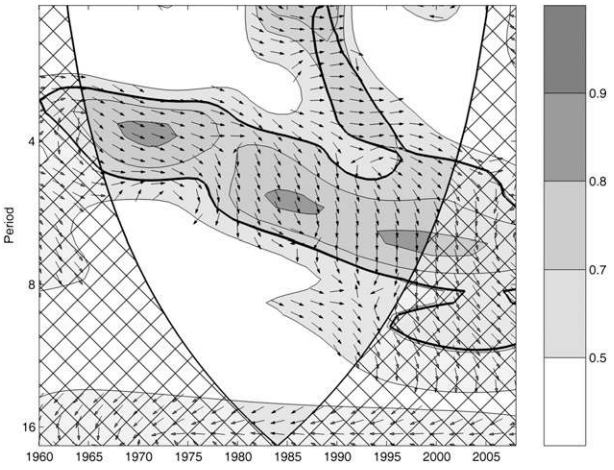

FIG. 3. The WTC of RTY over the WNP and the Niño-3 index during the period May–November. The cross-hatch indicates regions inside the COI and the thick black contour indicates 95% confidence level. The arrows indicate the relative phase relationship, with pointing right representing in-phase, pointing left representing antiphase, and pointing straight down indicating the lead of RTY by 90°.

between two phenomena (Gurley and Kareem 1999; Gurley et al. 2003), and their significant linear correlation relationship, if it is real, should thus be shown in WTC analyses as well. Unlike cross-wavelet transform, it is always helpful to implement the WTC analysis for relationship studies, even at intervals where high coherence exists but only minimal power is shown in the WPS of the two processes.

Following Grinsted et al. (2004), WTC can simply be defined by normalizing the wavelet cross spectrum to the single WPS, and WTC squared is thus

$$R^2(x,y) = \frac{|\varsigma[W(x,y)]|^2}{\varsigma[W(x)] \times \varsigma[W(y)]}, \tag{4}$$

where the W operator is the continuous wavelet transform when it has one argument and cross-wavelet transform when it has two, and $\varsigma = S \cdot s^{-1}$, in which S is the smoothing operator that helps strike a balance between resolution and significance. Because of the normalizing nature of WTC, the bias problem exists in WPS and wavelet cross spectrum does not occur in WTC. The same applies for PWC and MWC. The term "coherence" usually stands for the WTC squared, which ranges from 0 to 1 (1 being the highest coherence), given by smoothing operators. Monte Carlo methods are used to determine the statistical significance level of WTC.

The time series of the first PC of 850-hPa relative vorticity (RV1), that of 200–850-hPa vertical wind shear of zonal wind (VWS1), and the second PC of moist static energy (MSE2) are highly correlated with RTY and the Niño-3 index at a >95% confidence level with correlation coefficients of >0.37 and >0.57, respectively. These time series provide a demonstration of the application of WTC (Fig. 2). For example, the WTC of RTY and RV1 suggests that the two series have apparent coherence throughout the study period around the 3–16-yr band, where the mean phase of oscillations within the significant regions and outside COI is ~32°. The WTC of RTY and VWS1 and of RTY and MSE2 implies that their relationships are dominant only after the mid-1980s around the 4–16-yr band, in which the corresponding mean phase angles Φ_m are ~14° and ~27°, respectively. The in-phase relationships agree with the positive correlation coefficients found by simple correlations and suggest that stronger low-level relative vorticity is associated with an increase in tropical cyclone activity, while the vertical wind shear of the zonal wind and moisture static energy also contribute after the mid-1980s. This example shows the usefulness of WTC in determining the varying phases and intermittent correlation relationships between two phenomena.

4. PWC

Since RTY appears to be related to ENSO at around the 2–8-yr band (Fig. 3) and the time series of RV1, VWS1, and MSE2 are all significantly correlated with the Niño-3 index, the "stand-alone" relationship between RTY and

the PCs should be studied by removing the effect of ENSO. Partial correlation is one of the methods that can be used in a simple correlation concept. In wavelet applications, we can perform this with the help of PWC.

PWC is a technique similar to partial correlation that helps find the resulting WTC between two time series y and x_1 after eliminating the influence of the time series x_2. As WTC has a working principle similar to that of the traditional correlation coefficient, it can thus be understood as a localized correlation in the time–frequency space (Grinsted et al. 2004). WTC between y and x_1, y and x_2, and x_1 and x_2 is written as

$$
\begin{aligned}
R(y,x_1) &= \frac{\mathrm{s}[W(y,x_1)]}{\sqrt{\mathrm{s}[W(y)]\cdot \mathrm{s}[W(x_1)]}};\\
R^2(y,x_1) &= R(y,x_1)\cdot R(y,x_1)^*;\\
R(y,x_2) &= \frac{\mathrm{s}[W(y,x_2)]}{\sqrt{\mathrm{s}[W(y)]\cdot \mathrm{s}[W(x_2)]}};\\
R^2(y,x_2) &= R(y,x_2)\cdot R(y,x_2)^*;\\
R(x_2,x_1) &= \frac{\mathrm{s}[W(x_2,x_1)]}{\sqrt{\mathrm{s}[W(x_2)]\cdot \mathrm{s}[W(x_1)]}};\\
R^2(x_2,x_1) &= R(x_2,x_1)\cdot R(x_2,x_1)^*. \qquad (5)
\end{aligned}
$$

Mihanović et al. (2009) extended the concept from simple linear correlation and suggested that the PWC squared (after the removal of the effect of x_2) can be defined by an equation similar to the partial correlation squared, as

$$
RP^2(y,x_1,x_2) = \frac{|R(y,x_1) - R(y,x_2)\cdot R(y,x_1)^*|^2}{[1-R(y,x_2)]^2[1-R(x_2,x_1)]^2}, \qquad (6)
$$

which is like the simple WTC, ranging from 0 to 1.

In this case, a low PWC squared shown at where a high wavelet coherence squared was found implies that the time series x_1 does not have significant influence on the time series y at that particular time–frequency space, and time series x_2 dominates the effect on the variance of y, and vice versa for the opposite case. If both $RP^2(y,x_1,x_2)$ and $RP^2(y,x_2,x_1)$ still have significant bands, both x_1 and x_2 have a significant influence on y. The coherences calculated with this technique, consistent with WTC, as well as the MWC to be discussed in section 5 do not rely on the magnitude of the input time series. Maraun and Kurths (2004) also pointed out that the wavelet transform of the realization of a mixing process could give a random number as an end product. In other words, two independent processes do not necessarily give zero coherence. Significance tests are therefore needed and, similar to WTC, Monte Carlo methods are used for

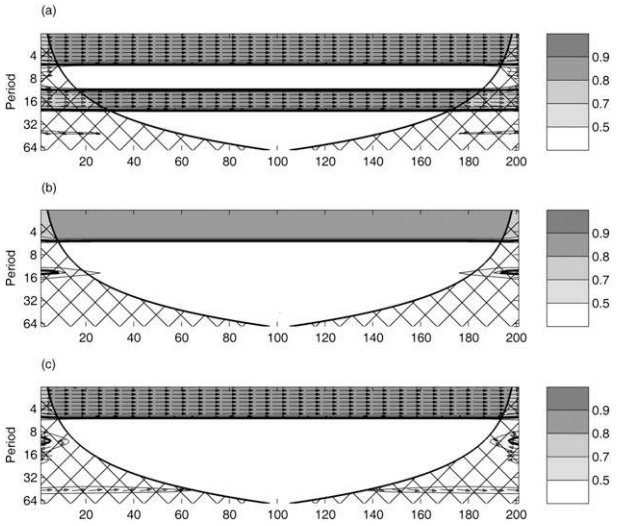

FIG. 4. (a) The WTC between an artificial time series comprising sine waves of six different periods (1, 4, 8, 16, 32, and 64 yr) and that of two different periods (4 and 16 yr). (b) The PWC of the two artificial time series used in (a), after the removal of a time series of sine wave with a period of 16 yr. (c) Similar to (a), but for the time series comprising sine waves of the five different periods and a time series of a sine wave with the period of 4 yr only. The cross-hatching indicates regions inside the COI and the thick black contour indicates 95% confidence level. The arrows indicate the relative phase relationship, with those pointing right representing in-phase.

PWC. The effect of PWC is shown using ideal signals in Fig. 4b by removing the effect of a 16-yr-period sine wave time series from the WTC of an artificial time series comprising sine waves with six different periods (1, 4, 8, 16, 32, and 64 yr) and that consisting of two different periods (4 and 16 yr) of sine waves (Fig. 4a). The resulting PWC squared, which should ideally show significant bands at a 4-yr period only, is comparable to the WTC of the time series of sine waves with the five different periods and a 4-yr-period sine wave time series (Fig. 4c).

The squared PWCs of RTY and RV1, RTY and VWS1, and RTY and MSE2 over the WNP (after the removal of the ENSO effect) are shown in Fig. 5. The stand-alone coherence relationships between them can be reanalyzed with these squared PWCs. Substantial reductions in the amplitude and areal extent of the previously found WTC squared (Fig. 2), especially for interannual variations, are observed. Except for the significant region present in the squared PWC of RTY and RV1 around the 8–10-yr band, where RTY does not seem to be related to ENSO (Fig. 3), almost all the significant regions have disappeared. The reductions imply that there is a significant contribution of the ENSO effect to the relationship between RTY and the large-scale parameters. This is evident that the variability of tropical cyclone activity is forced by ENSO via

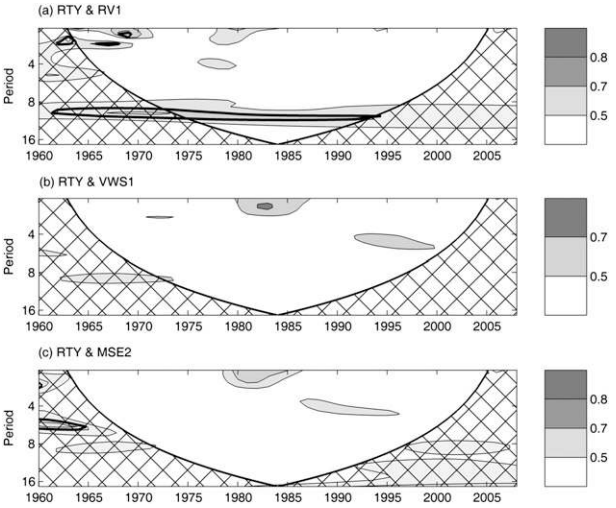

FIG. 5. The PWCs of (a) RTY and RV1, (b) RTY and VWS1, and (c) RTY and MSE2 during the period May–November (after the removal of ENSO effect). The cross-hatching indicates regions inside the COI and the thick black contour indicates 95% confidence level.

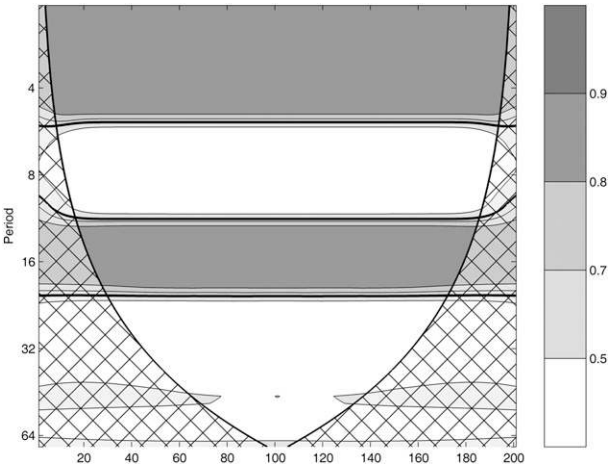

FIG. 6. The MWCs of an artificial time series comprising sine waves of six different periods (1, 4, 8, 16, 32, and 64 yr), a time series of sine waves with a 4-yr period, and a time series of sine waves with a 16-yr period. The cross-hatching indicates regions inside the COI and the thick black contour indicates 95% confidence level.

the alteration of the atmospheric circulation, as suggested by Chan and Liu (2004).

5. MWC

Akin to PWC, MWC works like multiple correlation that is capable of seeking the resulting coherence of multiple independents on a dependent. Because of the similar nature between correlation coefficients and WTC, using the WTC between y and x_1, y and x_2, and x_1 and x_2 calculated in (5), the application of MWC can be defined with the following equation:

$$RM^2(y,x_2,x_1)=\frac{R^2(y,x_1)+R^2(y,x_2)-2\mathrm{Re}[R(y,x_1)\cdot R(y,x_2)^*\cdot R(x_2,x_1)^*]}{1-R^2(x_2,x_1)}, \quad (7)$$

which gives the resulting wavelet coherence squared that computes the proportion of wavelet power of the dependent time series y that is explainable by the two independents x_1 and x_2 at a given time and frequencies. The significant levels are again calculated with the Monte Carlo method (Mihanović et al. 2009). Since MWC is very sensitive to the dependencies of time series, the assurance of the independence of x_1 and x_2 is a must before carrying out MWC. Otherwise, results with exceptionally high coherence may be produced. The MWCs of an artificial time series comprising sine waves of six different periods (1, 4, 8, 16, 32, and 64 yr), a time series of sine waves with a 4-yr period, and a time series of sine waves with a 16-yr period are shown in Fig. 6.

Other than the canonical ENSO, the ENSO Modoki is also found to possess obvious relationships with RV1, VWS1, and MSE2, with correlation coefficients >0.42 (>99% confidence level). The WTCs of the EMI and the PCs show significant dominant oscillations, mostly around the 8–16-yr band (not shown), which suggests that the ENSO Modoki may have a significant impact on the interdecadal variability of tropical cyclone activity. The WTC of the monthly Niño-3 index and EMI show only a few significant regions (Fig. 7), indicating that the canonical ENSO and Modoki ENSO are largely independent, which confirms the suggestion of Ashok et al. (2007) further *to all scales*. The application of MWC is therefore illustrated by investigating the composite effect of the canonical ENSO and ENSO Modoki on the variability of the PCs, respectively.

The combined impact of the canonical ENSO and ENSO Modoki on RV1 can be studied with MWC squared by putting RV1 as y and the Niño-3 index and the EMI as x_1 and x_2, respectively, in (7). A similar method can be used for investigating their effect on VWS1 and MSE2. The squared MWC of RV1, the Niño-3 index, and the EMI; VWS1, the Niño-3 index, and the EMI; and MSE2, the Niño-3 index, and the EMI are shown in

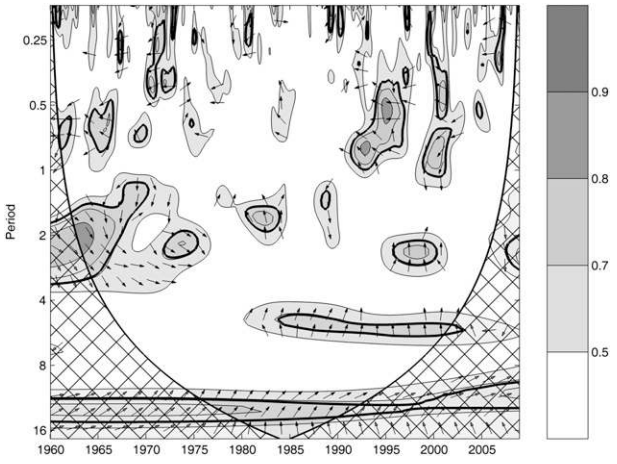

FIG. 7. The WTC of monthly Niño-3 index and EMI. Monthly climatological means of each month are removed from the datasets. The cross-hatching indicates regions inside the COI and the thick black contour indicates 95% confidence level. The arrows indicate the relative phase relationship, with those pointing right representing in-phase, pointing left representing antiphase, and pointing straight down indicating the lead of Niño-3 index by 90°.

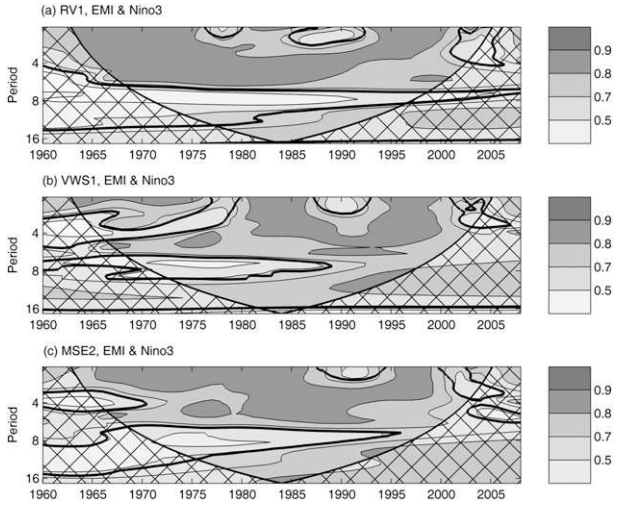

FIG. 8. The MWCs of (a) RV1, EMI, and Niño-3 index, (b) VWS1, EMI, and Niño-3 index, and (c) MSE2, EMI, and Niño-3 index during the period May–November. The cross-hatching indicates regions inside the COI and the thick black contour indicates 95% confidence level.

Fig. 8. Significant regions can all be seen on almost the entire spectra, which suggests that the usefulness of MWC in identifying the variability of the large-scale parameters PCs together with those of the Niño-3 index and the EMI. This is because the Niño-3 index is likely to account for the reflection of interannual variability and the EMI for the interdecadal variability, at least statistically, according to their squared WTC with those PCs. Further investigation of the EOF patterns is needed for a physical explanation of such dependencies.

With MWC, by comparing different combinations of the independent variables, the combination that best represents the dependent one may also be found. For example, as a significant relationship exists between VWS1 and the DMI, with a correlation coefficient of 0.40 (>95% confidence level), by comparing the squared MWC of VWS1, the DMI, and the Niño-3 index (Fig. 9) with that of VWS1, the EMI, and the Niño-3 index (Fig. 8b), the areal extent and amplitude of significant regions of the former are not comparable to those of the latter. This infers that EMI and the Niño-3 index together provide a better explanation of the variability of VWS1 than using the DMI and the Niño-3 index. Even worse results are found for the combination of the DMI and the EMI (not shown). This example demonstrates the usefulness of MWC in model simulations in helping to find the best group of predictors that explain the predictand *on all scales*.

6. Discussion and summary

The present study demonstrates the applications of PWC and MWC. The possible ENSO-related impact of the large-scale atmospheric factors leading the variability of tropical cyclone activity over the WNP is used as an example. PWC is a technique similar to partial correlation that helps find the resulting WTC between two time series after eliminating the influence of their common dependence, while MWC, working like multiple correlation, is useful in seeking the resulting WTC of

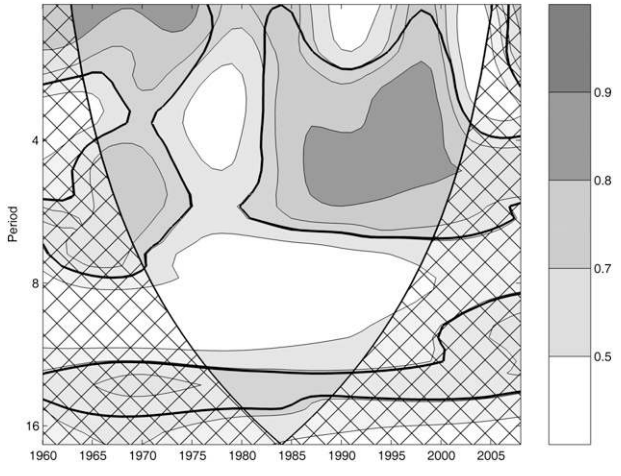

FIG. 9. The MWC of VWS1, DMI, and the Niño-3 index during the period May–November. The cross-hatching indicates regions inside the COI and the thick black contour indicates 95% confidence level.

multiple independents on a dependent. Given the similar working principle to that of traditional correlation coefficients, WTC can be seen as a localized correlation in a time–frequency space (Grinsted et al. 2004). PWC and MWC can therefore be defined easily with the concepts of partial and multiple correlation, as suggested by Mihanović et al. (2009).

With wavelet analysis, the problem of studying nonstationary time series has been much improved compared to Fourier transform, and one may now be able to study the variations of phenomena in a time–frequency space. However, imperfections of this tool cannot be neglected. First, because wavelet analysis is an expansion of a one-dimension time series, like simple correlation, the domain selection for analysis is very critical. In other words, the existence of noise is almost inevitable. This error may even be magnified when undergoing a time–frequency expansion. For example, the domain for large-scale parameters chosen in this study may not have consistent relationships with RTY and averaging across the domain could disrupt the relationships. Second, as wavelet analysis is developed mainly for studying periodicity, even though phase angle may help validate relationships, conclusions should not be drawn about relationships without any expectation of further investigation. Significant coherence could result even for random signals that happen to oscillate at the same frequency at particular intervals simultaneously. On the other hand, although angular standard deviation[2] measures the scattering of phase angle and may be able to test the credibility of angle mean, a large circular standard deviation does not necessarily imply doubts to that significant region and thus to the possible relationship between those phenomena. As long as the phase angles do not have sudden changes in the significant regions, as mentioned in section 3b, the possible physical relationship revealed may still be applicable.

To conclude, PWC and MWC further expand the applications of wavelet analysis, which helps diagnose the time series in a time–frequency space. They should have wide applications in the study of geophysical systems, for both observational and modeling ones, where trends and periodicities of oscillations with various frequencies are often investigated.

Acknowledgments. Special thanks to T. W. Kwok for his help in developing the software package. The wavelet software was provided by C. Torrence and G. Compo (see online at http://paos.colorado.edu/research/wavelets/), while the cross-wavelet and wavelet coherence software, from which some part of the code is used in ours, were provided by A. Grinsted (see online at http://www.pol.ac.uk/home/research/waveletcoherence).

[2] Note that $\sigma_\Phi = \sqrt{-2\ln(R/n)}$, where $X = \sum_{n=1}^{N} \cos(\Phi_n)$, $Y = \sum_{n=1}^{N} \sin(\Phi_n)$, and $R = \sqrt{(X^2 + Y^2)}$ (Zar 1999).

APPENDIX

List of Symbols and Acronyms

List of symbols	
Continuous wavelet transform on time series a_n	W_n^A, $W(a)$
Cross-wavelet power of times series a_n and b_n	$\lvert W_n^{AB}\rvert$
Mean phase angle	Φ_m
Multiple wavelet coherence of time series b_n and two independents $a1_n$ and $a2_n$	$RM(b, a_1, a_2)$
Partial wavelet coherence of times series $a1_n$ and b_n (after the removal of time series $a2_n$)	$RP(a_1, b, a_2)$
Phase difference	Φ_n
S including the weighing by s^{-1}	$\mathfrak{s}$
Scale level	j
Set of time scales used	s
Smoothing operator	S
Time step	δt
Wavelet coherence of times series a_n and b_n	$R(a, b)$
Wavelet function	ψ_0

List of acronyms	
COI	Cone of influence
DMI	Indian Ocean dipole model index
EMI	ENSO Modoki index
ENSO	El Niño–Southern Oscillation
EOF	Empirical orthogonal function
IBTrACS	International Best Track Archive for Climate Stewardship
MSE2	The time series of the second PC of moist static energy
MWC	Multiple wavelet coherence
NOAA	National Oceanic and Atmospheric Administration
PWC	Partial wavelet coherence
PC	Principal component
RTY	Ratio of number of typhoons to number of tropical cyclones
RV1	The time series of the first PC of 850-hPa relative vorticity
VWS1	The time series of the first PC of 200–850-hPa vertical wind shear of zonal wind
WNP	Western North Pacific
WPS	Wavelet power spectrum
WTC	Wavelet coherence

REFERENCES

Allen, M. R., and L. A. Smith, 1996: Monte Carlo SSA: Detecting irregular oscillation in the presence of colored noise. *J. Climate,* **9,** 3373–3404.

Ashok, K., S. Behera, A. S. Rao, H. Y. Weng, and T. Yamagata, 2007: El Niño Modoki and its possible teleconnection. *J. Geophys. Res.,* **112,** C11007, doi:10.1029/2006JC003798.

Chan, J. C. L., 2009: Thermodynamic control on the climate of intense tropical cyclones. *Proc. Roy. Soc. A,* **465,** 3011–3021.

——, and K. S. Liu, 2004: Global warming and western North Pacific typhoon activity from an observational perspective. *J. Climate,* **17,** 4590–4602.

Chen, G., and C.-Y. Tam, 2010: Different impacts of two kinds of Pacific Ocean warming on tropical cyclone frequency over the western North Pacific. *Geophys. Res. Lett.,* **37,** L01803, doi:10.1029/2009GL041708.

Daubechies, I., 1992: *Ten Lectures on Wavelets.* Society for Industrial and Applied Mathematics, 357 pp.

Emanuel, K. A., 2005: Increasing destructiveness of tropical cyclones over the past 30 years. *Nature,* **436,** 686–688.

Gilman, D. L., F. J. Fuglister, and J. M. Mitchell, 1963: On the power spectrum of ''red noise.'' *J. Atmos. Sci.,* **20,** 182–184.

Gray, W. M., 1979: Hurricanes: Their formation, structure, and likely role in the tropical circulation. *Meteorology over the Tropical Oceans,* D. B. Shaw, Ed., Royal Meteorological Society, 155–218.

Grinsted, A., J. C. Moore, and S. Jevrejeva, 2004: Application of the cross wavelet transform and wavelet coherence to geophysical time series. *Nonlinear Processes Geophys.,* **11,** 561–566.

Gurley, K., and A. Kareem, 1999: Applications of wavelet transforms in earthquake, wind and ocean engineering. *Eng. Struct.,* **21,** 149–167.

——, T. Kijewski, and A. Kareem, 2003: First- and higher-order correlation detection using wavelet transforms. *J. Eng. Mech.,* **129,** 188–201.

Kalnay, E., and Coauthors, 1996: The NCEP/NCAR 40-Year Reanalysis Project. *Bull. Amer. Meteor. Soc.,* **77,** 437–471.

Knapp, K. R., M. C. Kruk, D. H. Levinson, H. J. Diamond, and C. J. Neumann, 2010: The International Best Track Archive for Climate Stewardship (IBTRACS). *Bull. Amer. Meteor. Soc.,* **91,** 363–376.

Knutson, T. R., and R. E. Tuleya, 1999: Increased hurricane intensities with CO_2-induced warming as simulated using the GFDL hurricane prediction system. *Climate Dyn.,* **15,** 503–519.

Kruk, M. C., K. R. Knapp, and D. H. Levinson, 2010: A technique for combining global tropical cyclone best track data. *J. Atmos. Oceanic Technol.,* **27,** 680–692.

Liu, Y., X. S. Liang, and R. H. Weisberg, 2007: Rectification of the bias in the wavelet power spectrum. *J. Atmos. Oceanic Technol.,* **24,** 2093–2102.

Maraun, D., and J. Kurths, 2004: Cross wavelet analysis: Significance testing and pitfalls. *Nonlinear Processes Geophys.,* **11,** 505–514.

Mihanović, H., M. Orlić, and Z. Pasrić, 2009: Diurnal thermocline oscillations driven by tidal flow around an island in the Middle Adriatic. *J. Mar. Syst.,* **78,** S157–S168.

Ng, E. K. W., and J. C. L. Chan, 2012: Interannual variations of tropical cyclone activity over the north Indian Ocean. *Int. J. Climatol.,* **32,** 819–830, doi:10.1002/joc.2304.

Torrence, C., and G. P. Compo, 1998: A practical guide to wavelet analysis. *Bull. Amer. Meteor. Soc.,* **79,** 61–78.

Veleda, D., R. Montagne, and M. Araújo, 2012: Cross-wavelet bias corrected by normalizing scales. *J. Atmos. Oceanic Technol.,* **29,** 1401–1408.

Webster, P. J., G. J. Holland, J. A. Curry, and H.-R. Chang, 2005: Changes in tropical cyclone number, duration, and intensity in a warming environment. *Science,* **309,** 1844–1846.

Xue, Z., and C. J. Neumann, 1984: Frequency and motion of western North Pacific tropical cyclones. NOAA Tech. Memo. NWS NHC 23, 89 pp.

Zar, J. H., 1999: *Biostatistical Analysis.* Prentice Hall, 601 pp.